Solid State Ionics 301 (2017) 133–137

Contents lists available at ScienceDirect

Solid State Ionics

journal homepage: www.elsevier.com/locate/ssi

Structural stability and Li-ion transport property of $LiFePO_4$ under high-pressure

Haini Dong [a,b,1], Hao Guo [c,1], Yu He [a,*], Jian Gao [d], Wenze Han [c,*], Xia Lu [e], Shuai Yan [f], Ke Yang [f], Heping Li [a], Dongfeng Chen [c], Hong Li [d]

[a] Key Laboratory of High-Temperature and High-Pressure Study of the Earth's Interior, Institute of Geochemistry, Chinese Academy of Sciences, Guiyang, Guizhou 550081, China
[b] Center for High Pressure Science and Technology Advanced Research, Shanghai 201203, China
[c] China Institute of Atomic Energy, Beijing 102413, China
[d] Beijing National Laboratory for Condensed Matter Physics, Institute of Physics, Chinese Academy of Sciences, Beijing 100190, China
[e] College of Energy, Beijing University of Chemical Technology, Beijing 100029, China
[f] Shanghai Synchrotron Radiation Facility (SSRF), Shanghai Institute of Applied Physics, Chinese Academy of Science, Shanghai 201800, China

ARTICLE INFO

Article history:
Received 9 January 2017
Accepted 31 January 2017
Available online xxxx

Keywords:
$LiFePO_4$
High-pressure
In-situ XRD
In-situ Raman spectroscopy
Li-ion transport property

ABSTRACT

$LiFePO_4$ with olivine structure is an intensively investigated cathode material for lithium ion batteries. However, the relationship between lattice parameters and Li-ion transport property has not been concerned previously. In this work, pristine $LiFePO_4$ nanoparticle was synthesized by hydrothermal method. *In-situ* high-pressure synchrotron X-ray diffraction (XRD), *in-situ* Raman spectroscopy and first-principles calculations were used to characterize the structure evolution of $LiFePO_4$ from ambient pressure to 21.5 GPa and obtain its equation of state and bulk modulus. Unlike previously reported phase transition of $LiFePO_4$ from olivine structure to β′ phase (symmetry group *Cmcm*) under high pressure and high temperature, we did not observe any phase transition at pressure below 21.5 GPa. Here, the lattice parameters show an anisotropic decreasing as pressure increases, and Li—O bonds are much more compressible than Fe—O and P—O bonds during compression. The Li^+ migration barrier energy of $LiFePO_4$ under pressure was further investigated by first-principles calculations. The barrier energy along [010] and [001] directions increases with applied pressure, and the one-dimensional ionic diffusion property of $LiFePO_4$ remains at the pressure below 28.2 GPa. These findings will enhance our understanding on this important cathode material and provide hints on materials synthesis and modification by high-pressure technology.

1. Introduction

Olivine structured $LiFePO_4$ with a high theoretical capacity of 170 mAh/g is considered as a promising cathode material of lithium-ion batteries for electric vehicles due to its high safety, low cost, thermal stability and environmentally benign properties [1,2]. However, due to the low intrinsic electronic and ionic conductivities, batteries with $LiFePO_4$ cathode often exhibit low power density [3,4]. Techniques, such as carbon coating and decreasing the particle size, were effectively used to improve the electrochemical performance of $LiFePO_4$ [5–8]. On the other hand, experimental and theoretical methods were used to clarify Li^+ transport mechanism of $LiFePO_4$. First-principles nudged elastic band calculations predicted Li^+ migrates along [010] direction in the lattice of $LiFePO_4$ [9,10]. This one-dimensional diffusion model was confirmed by neutron diffraction experiment [11]. Further investigation on the structural and Li^+ migration properties of $LiFePO_4$ will certainly bring more inspirations on the material design for lithium ion batteries.

Olivine $LiFePO_4$ shows a phase transition to a polymorph (β′ phase) with *Cmcm* symmetry group at the pressure of 6.5 GPa and the temperature of 900 °C [12]. Ashton et al. compared their Li^+ diffusion coefficient using muon spectroscopy. The high-pressure structure exhibits higher Li^+ diffusion coefficient. It seems that high-pressure modification or phase transition may benefit Li-ion migration in $LiFePO_4$. However, the electrochemical performance of β′-$LiFePO_4$ cathode is very poor [13]. In order to specifically study the structural modification and the change of Li-ion transport property under pressure, here, the structural evolution of $LiFePO_4$ from ambient pressure to 21.5 GPa was investigated by *in-situ* X-ray diffraction and *in-situ* Raman spectroscopy in a diamond anvil cell at room temperature, and the Li^+ migration barrier energy along [010] and [001] directions under different pressure was calculated by first-principles method. Moreover, some fundamental properties of $LiFePO_4$, such as equation of state, bulk modulus and the cell parameters evolution under

* Corresponding authors.
E-mail addresses: heyu@mail.gyig.ac.cn (Y. He), hanwenze2003@163.com (W. Han).
[1] These authors contributed equally.

http://dx.doi.org/10.1016/j.ssi.2017.01.026
0167-2738/

pressure, will be provided by the synchrotron radiation experiments. The fully investigation on the relationship between structural and ion migration property will enhance our understanding on this important cathode material and provide hints on materials synthesis and modification using high-pressure technology. In addition, this fundamental study will help to justify if $LiFePO_4$ is suitable for applying on devices working under extreme conditions, such as deep-sea and deep-earth explorations.

2. Experimental

2.1. Sample preparation

$LiFePO_4$ powders were prepared by hydrothermal process [14,15]. The starting materials were $LiOH \cdot H_2O$ (99%, Adamas Reagent Co., Ltd.), $FeSO_4 \cdot 7H_2O$ (99.5%, J&K Scientific Ltd.), H_3PO_4 (85% solution, J&K Scientific Ltd.) and ascorbic acid (99%, J&K Scientific Ltd.). Ascorbic acid, H_3PO_4 and $FeSO_4 \cdot 7H_2O$ powders were added to distilled water under stirring. Then 1 M LiOH solution was slowly added to the solution. The molar ratio of the Li^+:Fe^{2+}:PO_4^{3-} in the precursor solution was controlled to be 3:1:1. A Teflon obturation vessel filled with the mixture was sealed in a stainless steel autoclave and heated at 180 °C for 10 h, followed by being cooled down to room temperature naturally. Precipitates were collected by suction filtration and washed with deionized water and alcohol. After dried at 80 °C for 1 h in the vacuum oven, light green powder was collected and then heated at 800 °C for 5 h in Ar-H_2 atmosphere (H_2 5%).

2.2. Sample characterization

The X-ray diffraction (XRD) measurement was carried out on a Bruker D8 Advance diffractometer using a CuKa radiation source ($\lambda_1 = 1.5406$ Å, $\lambda_2 = 1.54439$ Å). XRD patterns were collected by a step-scanning mode in the range of 15–80°.

In-situ high-pressure angle-dispersive XRD experiments with a wavelength of 0.6199 Å and a focused beam size of approximately 3×4 mm^2 were performed at beamline 15U1 of Shanghai Synchrotron Radiation Facility (SSRF). Mao-type symmetric diamond anvil cell with 300 mm culet size was used to generate high pressure. The T301 stainless gasket was pre-indented to ~40 mm in thickness, and a hole of 100 mm diameter was drilled in the center as sample chamber. Silicon oil was loaded as pressure-transmitting medium. The samples were grounded to fine powders, and then were loaded into the hole along with a tiny ruby all beside the sample as a pressure calibrant. Rietveld structural refinements were employed for accurate phase analysis using GSAS software. *In-situ* high-pressure Raman spectroscopy was measured with a 532 nm laser. Pressure was calibrated by the ruby fluorescence method.

2.3. Theoretical calculation

The first-principles calculations were based on the Density Functional Theory (DFT) [16,17] within the Local Density Approximation (LDA) and Generalized Gradient Approximation (GGA) [18,19]. Considering the strongly correlated nature of the Fe 3d electrons a Hubbard-type correction U was taken into account [20,21]. According to a previous work, the effective U value was set to 4.3 eV [22]. All computations were carried out by the Vienna *Ab Initio* Simulation Package (VASP) [23]. In our calculations, a plane wave representation for the wave function with a cut off energy of 500 eV was adopted. Geometry optimizations were performed by using a conjugate gradient minimization until all the forces acting on ions were less than 0.01 eV/Å per atom. The calculation model was based on the primitive cell of $LiFePO_4$. The fully relaxed structure was treated as the structure at zero pressure. K-point mesh with a spacing of *ca.* 0.03 Å^{-1} was adopted. The relaxed structure calculations were performed at various constant volumes and the energy − volume data were fitted to a third-order Birch–Murnaghan equation of state (EOS):

$$E(V) = E_0 + \frac{9V_0B_0}{16}\left\{\left[\left(\frac{V_0}{V}\right)^{\frac{2}{3}} - 1\right]^3 B_0' + \left[\left(\frac{V_0}{V}\right)^{\frac{2}{3}} - 1\right]^2 \left[6 - 4\left(\frac{V_0}{V}\right)^{\frac{2}{3}}\right]\right\}, \quad (1)$$

where E_0 denotes the intrinsic energy at zero pressure, V_0 is the volume at zero pressure, B_0 is the bulk modulus and B_0' the first pressure derivative of the bulk modulus. The relation between the pressure and the volume at zero Kelvin degree can be expressed as:

$$P(V) = \frac{3B_0}{2}\left[\left(\frac{V_0}{V}\right)^{\frac{7}{3}} - \left(\frac{V_0}{V}\right)^{\frac{5}{3}}\right]\left\{1 + \frac{3}{4}(B_0' - 4)\left[\left(\frac{V_0}{V}\right)^{\frac{2}{3}} - 1\right]\right\}. \quad (2)$$

Li^+ migration energy was calculated by Climbing-Image Nudged Elastic Band (CINEB) method [24]. This approach duplicated a series of images (five images in our calculations) between the starting point and the end point of migrating ion to simulate the intermediate states, with the positions of the starting point and the end point fixed. A larger supercell $1 \times 2 \times 2$ containing 112 atoms was used for simulation. For the larger supercell adopted in CINEB calculations, only the Γ point was adopted for k-point sampling to reduce the computational cost. The convergence check indicates that a denser k-mesh does not affect our conclusion qualitatively.

3. Results and discussion

3.1. Structural stability of $LiFePO_4$ under high-pressure

The as prepared sample is determined to be single-phase $LiFePO_4$ with an olivine structure from the powder diffraction experiment as shown in Fig. 1. The hydrothermal synthesized $LiFePO_4$ without carbon coating has similar lattice parameters to those previous reports (a = 10.3341 Å, b = 6.006 Å, and c = 4.6985 Å) and a unit cell volume of 291.62 Å^3. The difference between the measured and calculated XRD data is also exhibited in Fig. 1.

Fig. 2 shows the evolution of the XRD patterns for $LiFePO_4$ under high-pressure. No new Bragg maxima indicating a phase transition is observed up to 21.5 GPa. The structure of $LiFePO_4$ olivine is stable at room temperature and pressure below 21.5 GPa. The compression of

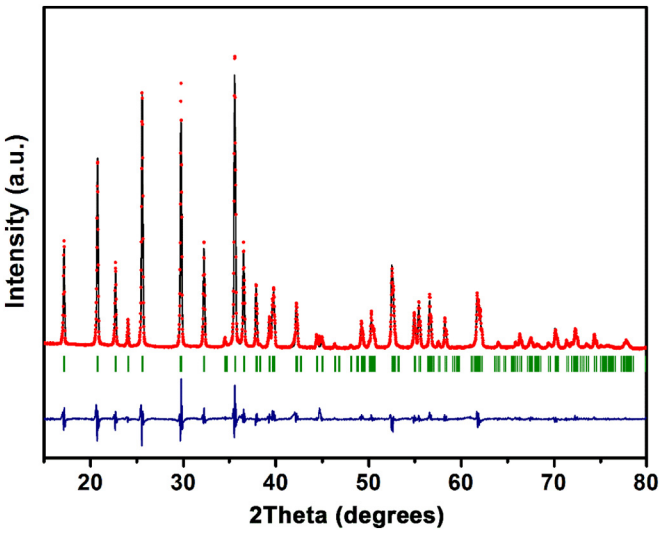

Fig. 1. Refinement of XRD data of $LiFePO_4$ at ambient conditions ($\lambda_1 = 1.5406$ Å, $\lambda_2 = 1.54439$ Å). Measured (black lines) and calculated (red dashed lines) patterns are shown, together with the difference curve (blue lines) and calculated positions of Bragg reflections (green tick marks). (For interpretation of the references to colour in this figure legend, the reader is referred to the web version of this article.)

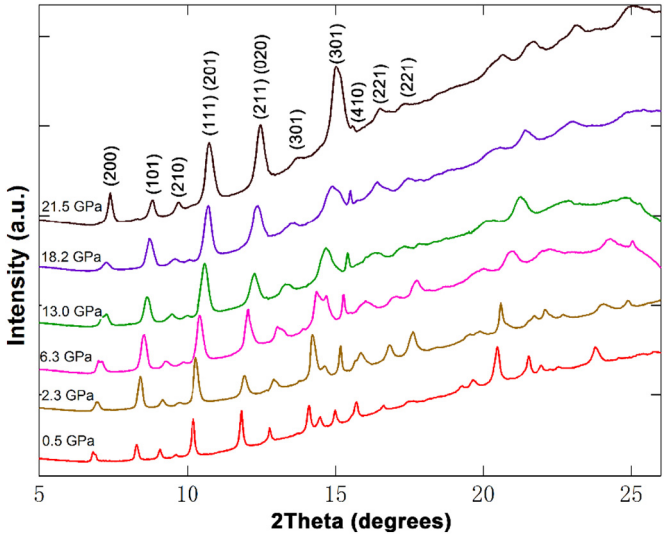

Fig. 2. *In situ* synchrotron XRD patterns of $LiFePO_4$ under compression from 0.5 GPa to 21.5 GPa.

the structure leads to the shift of the peaks toward higher degree and the typical broadening of the diffraction peaks. It is well-known that several olivine-like compounds transform into denser structures under high-pressure. The olivine-spinel phase transition under stress is observed in many compounds, such as Mg_2SiO_4, Fe_2SiO_4 and Mg_2GeO_4 [25,26]. Unlike these compounds listed above, $LiFePO_4$ and $LiNiPO_4$ undergo a phase transition from olivine structure to β′ phase (symmetry group *Cmcm*) at high pressure and high temperature [13]. However, the high-pressure phase β′-$LiFePO_4$ was not observed in our experiment due to the low ionic mobility for redistribution of atoms at room temperature.

In-situ Raman spectroscopy was employed to characterize the local structure changes of $LiFePO_4$ upon compression up to 18.3 GPa. As shown in Fig. 3, the modes agree very well with the assignments reported previously [27,28]. The vibrational bands above 400 cm^{-1} are the typical intramolecular stretching motions of the phosphate anion. Three bands in the Raman spectrum of $LiFePO_4$ are observed between 1100 and 900 cm^{-1}. The very sharp band at 953 cm^{-1} is attributed to the A_g mode of V_1, while the two weaker bands are thought to belong

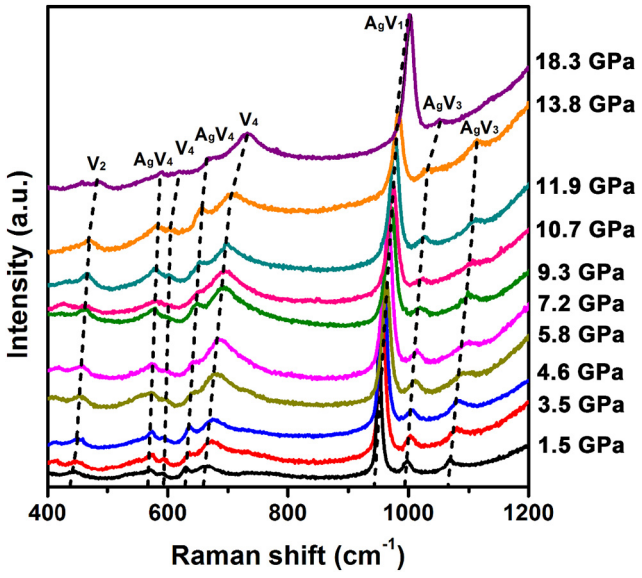

Fig. 3. *In-situ* Raman spectra of the $LiFePO_4$ upon compression at the range of 1.5–18.3 GPa in the frequency range of 400–1200 cm^{-1} at room temperature.

to the antisymmetric stretching modes of the PO^{-4} anion (V_3). Theory predicts V_4 to yield six Raman vibrations ($2A_g + B_{1g} + 2B_{2g} + B_{3g}$) and V_2 four Raman vibrations ($A_g + B_{1g} + B_{2g} + B_{3g}$) at the Brillouin zone center. The modes involving mostly V_4 motion are expected to occur at higher frequencies than those consisting primarily of V_2 motion. Six weak bands between 700 and 550 cm^{-1} are assigned to mostly V_4 vibrations with some contribution from V_2. A broad structure at ~444 cm^{-1} could be due to the overlapping of different bending modes of V_2. Upon compression to 18.3 GPa stepwise, all Raman bands of $LiFePO_4$ shift to higher frequencies with decreasing intensity and band broadening. The olivine structure of $LiFePO_4$ is persisted at pressure below 18.3 GPa. It is plausibly in consistence with the result of synchrotron XRD.

The cell volumes under different pressures are obtained by fitting the *in-situ* XRD data (Fig. 4). The pressure-volume relation can be fitted with third-order Birch –Murnaghan equation of state. The bulk modulus of $LiFePO_4$ olivine is determined to be 91.5 GPa with the first derivative (B_0') being fixed at 4. The equilibrated volume (V_0) is 292.38 $Å^3$ at zero pressure. The pressure-volume relation was also calculated by first-principles method (dot and dash lines in Fig. 4). The calculated pressure-volume relation is in a good agreement with the experimental date. However, the volume is a little bit overestimate for GGA + U, and a little bit underestimate for LDA + U. The calculated bulk moduli are 114.1 GPa (LDA + U) and 92.9 GPa (GGA + U) with V_0 equal to 300.62 $Å^3$ (LDA + U) and 292.38 $Å^3$ (GGA + U). Calculation with LDA + U better reflects the compressibility of $LiFePO_4$.

3.2. Anisotropic compressibility of $LiFePO_4$

The variation of experimental and calculated lattice parameters is compared in Fig. 5. Without extraordinary condition, the parameters decrease with applied pressure. The a, b and c are contracted to 9.62 Å, 5.73 Å and 4.47 Å at 21.5 GPa. In relative terms, the normalized contraction of a, b and c are 7.16%, 4.73% and 5.08% at 21.5 GPa respectively. It means the compression of $LiFePO_4$ is anisotropic. Lattice along [100] is more compressible than [010] and [001] directions. Similar results are given by DFT calculations.

In order to clarify the mechanism of anisotropic compression, the variations of calculated interatomic distance and polyhedral volume under pressure are compared in Fig. 6. At 20 GPa, the relative bond length change is 7.26% (Li—O), 4.66% (Fe—O) and 1.26% (P—O) respectively for GGA + U. The pressure-volume relations of LiO_6 octahedron, FeO_6 octahedron and PO_4 tetrahedron as shown in Fig. 6b exhibit a similar trends. The relative volume change is 17.73% (LiO_6), 12.38% (FeO_6)

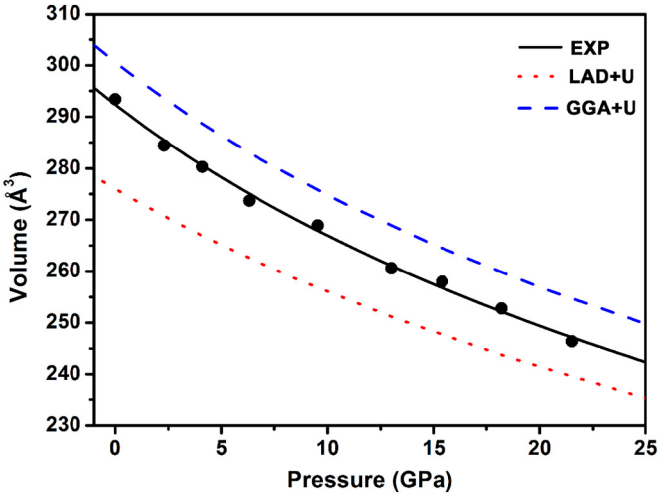

Fig. 4. The experimental and calculated pressure-volume diagram of olivine $LiFePO_4$, the black dots are obtained by *in situ* synchrotron XRD.

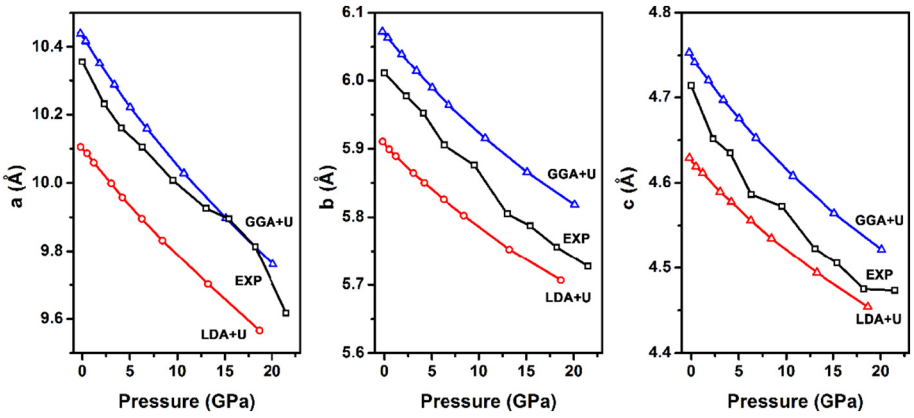

Fig. 5. The variation of lattice parameters of olivine $LiFePO_4$ under compression from experimental and calculated investigations.

and 3.92% (PO_4) for GGA + U. The same results are obtained from LDA + U calculations. It is obvious that Li—O bond is much more compressible than Fe—O and P—O bond, resulting high compressibility of LiO_6 octahedron. The different compressibility of bond length can give an explanation on the anisotropic compressibility of lattice parameters in $LiFePO_4$ structure.

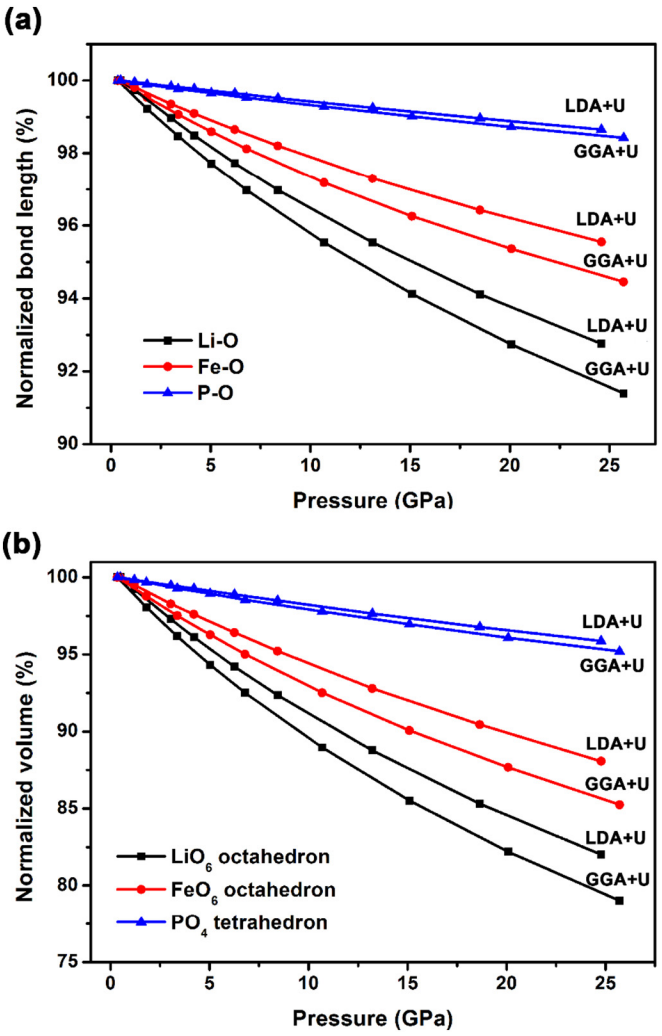

Fig. 6. (a) The calculated normalized bond length variation of Li—O, Fe—O and P—O. (b) Normalized volume change of LiO_6 octahedron, FeO_6 octahedron and PO_4 tetrahedron under high-pressure.

3.3. Li-ion migration barrier energy of $LiFePO_4$ under compression

There are three possible paths for Li^+ migration as shown in Fig. 7a. In order to investigate the Li^+ migration path and its migration energy under compression, the barrier energy of path 1 and path 2 is calculated by CINEB method. As Li^+ migration along path 3 is believed to be very hard and is difficult to study directly with the elastic band method [9], we did not calculate the migrate energy along path 3. At normal pressure, the migration barrier energy of path 1 and path 2 is 0.33 eV and 2.00 eV respectively. The much higher migration energy of path 2 prohibits its significant contribution to the Li^+ diffusion in $LiFePO_4$. However, the result is different from the experimental study on ionic transport of single crystalline $LiFePO_4$ [29,30]. In their work, the Li^+ conductivity along [010] and [001] are comparable and distinctly greater than along [100] indicating a two-dimensional Li^+ conduction in the b-c plane. They suggest that the obvious difference of experimental and theoretical study may be caused by the iron occupancy on the lithium site. Iron can block the diffusion of Li^+ in the channel along [010] direction. The Li-ion, which is blocked, may jump from one channel to another (along [001] direction) and leads to similar Li^+ conduction along [010] and [001] directions.

Upon compression, Li^+ migration barrier energy along [010] direction (path 1) in $LiFePO_4$ increases from 0.33 eV at 0.1 GPa (300.19 $Å^3$) to 0.58 eV at 28.2 GPa (245.59 $Å^3$) (Fig. 7b). The compression of the ion migration channel constrains Li^+ diffusion along [010] direction. On the other hand, the barrier energy is reduced by increasing the cell volume. When the cell volume is enlarged to 309.32 (−2.5 GPa) and 318.75 $Å^3$ (−4.8 GPa), the migration energy decreases to 0.31 and 0.30 eV respectively. The compression of cell lattice also confines Li^+ migration along [001] direction (path 2). Its migration energy increases from 2.00 eV at 0.1 GPa (300.19 $Å^3$) to 3.19 eV at 28.2 GPa (245.59 $Å^3$). The migration energy along [001] direction is still much higher under compression. It means that the one-dimensional Li^+ diffusion property of $LiFePO_4$ remains at the pressure below 28.2 GPa. The migration energy of path 2 also decreases obviously to 1.74 and 1.25 eV as the cell volume is enlarged to 309.32 (−2.5 GPa) and 318.75 $Å^3$ (−4.8 GPa). The anisotropic ionic conductivity in b-c plane is weaken in the enlarged cells.

Within expectation, the compression of $LiFePO_4$ cell lattice is unfavorable for Li^+ transport. Although the structure of $LiFePO_4$ is very stable at the pressure below 21.5 GPa, considering its one-dimensional ion diffusion property and the obvious increasing of migration energy under pressure, it is not suitable for devices of deep-sea and deep-earth explorations. On the other hand, the migration energy can be

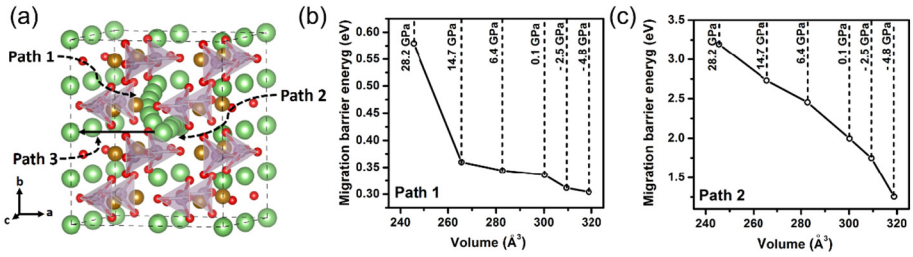

Fig. 7. (a) The possible Li^+ migration path in $LiFePO_4$ lattice. (b) The variation of calculated Li^+ migration barrier energy of path 1 (along [010] direction) at different cell volume (pressure). (c) The variation of calculated Li^+ migration barrier energy of path 2 (along [001] direction) at different cell volume (pressure).

reduced in an enlarged cell. As a result, in order to increase the ionic conductivity, larger cations and anions can be used as substitution to construct a larger framework of lattice. This inspiration can be helpful for material designs with high ionic conductivity for ionic devices.

4. Conclusion

High-pressure structural evolution of olivine $LiFePO_4$ was investigated by *in-situ* synchrotron X-ray diffraction (XRD), *in-situ* Raman spectroscopy and first-principles calculations. It is found that the olivine structure of $LiFePO_4$ could be maintained at the pressure below 21.5 GPa. Unlike previously reported high-pressure phase transition of $LiFePO_4$ from olivine to β' phase, no phase transition was observed in our experiments due to the low ionic mobility for overcoming the high kinetic barriers involved in a redistribution of atoms at room temperature. The bulk modulus of $LiFePO_4$ olivine was determined to be 91.5 GPa. The lattice parameters show an anisotropic decreasing as pressure increases. Upon compression, Li—O bonds are much more compressible than Fe—O and P—O bonds in olivine $LiFePO_4$, and lattice along [100] is more compressible than [010] and [001] directions. Similar structural properties under pressure are elucidated by DFT calculations. The calculation results on the ion migration properties of $LiFePO_4$ under high pressure show that Li^+ migration barrier energy along [010] and [001] directions increases with applied pressure, and the one-dimensional ionic diffusion property of $LiFePO_4$ remains at the pressure below 28.2 GPa. These findings will enhance our understanding on this important cathode material and provide hints on materials synthesis and modification by high-pressure technology.

Author contributions

The manuscript was written through contributions of all authors. All authors have given approval to the final version of the manuscript.

Notes

The authors declare no competing financial interest.

Acknowledgment

We acknowledge the support of Natural Science Foundation of China (Grant Nos. 51302259, 11205249), Science and Technology Program of Guizhou Province, China (SY [2013] 2284) and Excellence Fund Project of China Institute of Atomic Energy (Grant No. 16YC-201502). Prof. X. Lu thanks the funding resource from the State Key Laboratory of Organic-Inorganic Composites (oic-201701011). The authors are also grateful to Dr. Y. Sun for discussions.

References

[1] A.K. Padhi, K.S. Nanjundaswamy, J.B. Goodenough, J. Electrochem. Soc. 144 (1997) 1188.
[2] A. Yamada, S.C. Chung, K. Hinokuma, J. Electrochem. Soc. 148 (3) (2001) A224–A229.
[3] Z.H. Li, D.M. Zhang, F.X. Yang, J. Mater. Sci. 44 (2009) 2435.
[4] A.S. Anderesson, J.O. Thomas, J. Power Sources 97 (98) (2001) 498.
[5] N. Ravet, Y. Chouinard, J.F. Magnan, S. Besner, M. Gauthier, M. Armand, J. Power Sources 97-8 (2001) 503.
[6] B. Kang, G. Ceder, Nature 458 (2009) 190.
[7] P. Gibot, M. Casas-Cabanas, L. Laffont, S. Levasseur, P. Carlach, S. Hamelet, J.M. Tarascon, C. Masquelier, Nat. Mater. 7 (2008) 741–747.
[8] N. Meethong, H.-Y.S. Huang, W.C. Carter, Y.-M. Chiang, Electrochem. Solid-State Lett. 10 (2007) A134–A138.
[9] D. Morgan, A. Van der Ven, G. Ceder, Electrochem. Solid-State Lett. 7 (2004) A30.
[10] C.Y. Ouyang, S.Q. Shi, Z.X. Wang, X.J. Huang, L.Q. Chen, Phys. Rev. B 69 (2004) 104303.
[11] S. Nishimura, G. Kobayashi, K. Ohoyama, R. Kanno, M. Yashima, A. Yamada, Nat. Mater. 7 (2008) 707.
[12] O. Garcı'a-Moreno, M. Alvarez-Vega, F. Garcı'a-Alvarado, J. Garcı'a-Jaca, J.M. Gallardo-Amores, M.L. Sanjua'n, U. Amador, Chem. Mater. 13 (2001) 1570–1576.
[13] T.E. Ashton, J.V. Laveda, D.A. MacLaren, P.J. Baker, A. Porch, M.O. Jonesc, S.A. Corr, J. Mater. Chem. A 2 (2014) 6238.
[14] S. Yang, P.Y. Zavalij, M.S. Whittingham, Electrochem. Commun. 3 (2001) 505.
[15] X. Qin, X. Wang, H. Xiang, J. Xie, J. Li, Y. Zhou, J. Phys. Chem. C 114 (2010) 16806–16812.
[16] P. Hohenberg, W. Kohn, Phys. Rev. B 136 (1965) 864–871.
[17] W. Kohn, L. Sham, J. Phys. Rev. A 140 (1965) 1133–1138.
[18] D. Ceperley, B. Alder, Phys. Rev. Lett. 45 (1980) 566–569.
[19] J.P. Perdew, A. Zunger, Phys. Rev. B 23 (1981) 5048–5079.
[20] O. Bengone, M. Alouani, P. Blochl, J. Hugel, Phys. Rev. B 62 (2000) 16392.
[21] A.I. Liechtenstein, V.I. Anisimov, J. Zaanen, Phys. Rev. B 52 (1995) R5467.
[22] F. Zhou, M. Cococcioni, C.A. Marianetti, D. Morgan, G. Ceder, Phys. Rev. B 70 (2004) 235121.
[23] G. Kresse, J. Furthmüller, Phys. Rev. B 54 (1996) 11169–11186.
[24] G. Henkelman, B.P. Uberuaga, H. Jonsson, J. Chem. Phys. 113 (2000) 9901–9904.
[25] F.A.V. Meinesze, Nature 178 (1956) 1304.
[26] N.L. Ross, A. Navrotsky, Phys. Chem. Miner. 14 (1987) 473–481.
[27] C.M. Burba, R. Frech, J. Electrochem. Soc. 151 (2004) A1032–A1038.
[28] Y. Bai, Y. Yin, J. Yang, C. Qing, W. Zhang, J. Raman Spectrosc. 42 (2011) 831–838.
[29] R. Amin, P. Balaya, J. Maier, Electrochem. Solid-State Lett. 10 (1) (2007) A13.
[30] R. Amin, J. Maier, P. Balaya, D.P. Chen, C.T. Lin, Solid State Ionics 179 (2008) 1683–1687.